Published in final edited form as:
Eur J Nucl Med Mol Imaging. 2010 February ; 37(2): 339–348. doi:10.1007/s00259-009-1310-y.

Detection of hypoxia in microscopic tumors using ^{131}I-labeled iodo-azomycin galactopyranoside (^{131}I-IAZGP) digital autoradiography

Xiao-Feng Li,
Department of Medical Physics, Memorial Sloan-Kettering Cancer Center, New York, NY, USA; Imaging Center, The Fourth Affiliated Hospital of Harbin Medical University, Harbin, Heilongjiang, People's Republic of China; Department of Nuclear Medicine, The Second Affiliated Hospital of Harbin Medical University, Harbin, People's Republic of China; Department of Diagnostic Radiology, University of Louisville School of Medicine, 530 S. Jackson Street, CCB-C07, Louisville, KY 40202, USA

Xiaorong Sun,
Department of Medical Physics, Memorial Sloan-Kettering Cancer Center, New York, NY, USA, Department of Nuclear Medicine, PET-CT Center, Shandong Cancer Hospital and Institute, Jinan, Shandong, People's Republic of China

Yuanyuan Ma,
Department of Pathology, Memorial Sloan-Kettering Cancer Center, New York, NY, USA

Makiko Suehiro,
Department of Medical Physics, Memorial Sloan-Kettering Cancer Center, New York, NY, USA

Mutian Zhang,
Department of Medical Physics, Memorial Sloan-Kettering Cancer Center, New York, NY, USA

James Russell,
Department of Medical Physics, Memorial Sloan-Kettering Cancer Center, New York, NY, USA

John L. Humm,
Department of Medical Physics, Memorial Sloan-Kettering Cancer Center, New York, NY, USA

C. Clifton Ling, and
Department of Medical Physics, Memorial Sloan-Kettering Cancer Center, New York, NY, USA

Joseph A. O'Donoghue
Department of Medical Physics, Memorial Sloan-Kettering Cancer Center, New York, NY, USA

Xiao-Feng Li: xiao-feng.li@louisville.edu

Abstract

Purpose—Previous studies have shown that tumors less than 1 mm diameter derived from HT29 colorectal cancer cells are extremely hypoxic when grown intraperitoneally or intradermally in nude mice, whereas those of greater size (approximately 1–4 mm diameter) are not significantly hypoxic. The object of this study was to determine if digital autoradiography using the radiolabeled hypoxia imaging tracer iodo-azomycin galactopyranoside (^{131}I-IAZGP) could detect hypoxia in this model.

Correspondence to: Xiao-Feng Li, xiao-feng.li@louisville.edulinucmed@gmail.com.

Conflicts of interest None.

Methods—Microscopic HT29 tumors were grown as disseminated peritoneal disease and intradermally in nude mice. Tumors ranged in size from a few hundred microns to several millimeters in diameter. Animals were intravenously administered ^{131}I-IAZGP and pimonidazole 2 h before sacrifice. Following sacrifice, the intratumoral distribution of ^{131}I-IAZGP was assessed by digital autoradiography and compared with immunofluorescence microscopic images of pimonidazole binding and carbonic anhydrase IX (CAIX) expression.

Results—The distributions of ^{131}I-IAZGP, pimonidazole, and CAIX expression were similar. Tumors less than 1 mm diameter displayed high ^{131}I-IAZGP uptake; these tumors also stained strongly for pimonidazole and CAIX. Larger tumors (approximately 1–4 mm diameter) were not significantly hypoxic and had low ^{131}I-IAZGP accumulation.

Conclusion—^{131}I-IAZGP can detect hypoxia in microscopic tumors. Microscopic tumors are useful models for the validation of hypoxia radiotracers, and digital autoradiography is an appropriate technique for studying the distribution of hypoxia radiotracers in microscopic tumors.

Keywords

Micrometastasis; Tumor hypoxia; Iodo-azomycin galactopyranoside; Hypoxia radiotracer; Autoradiography

Introduction

We recently reported the existence of severe hypoxia in microscopic tumors derived from HT29 and HCT-8 colorectal cancer cell lines when grown intradermally or as disseminated intraperitoneal disease in animals [1,2]. Specifically, it was found that the smallest tumors (of submillimeter dimensions) were intensely hypoxic with little to no vasculature or blood perfusion. In contrast, somewhat larger tumors (of 1– 4 mm diameter) were typically well vascularized with significant blood perfusion and little to no detectable hypoxia. These observations were consistent with the hypothesis of a temporal progression in microscopic tumor development from an avascular hypoxic state to a vascular non-hypoxic state via a hypoxia-mediated “angiogenic switch” event.

Radiolabeled tracers such as ^{18}F-fluoromisonidazole (FMISO) [3–5], copper(II)-diacetyl-bis (*N*(4)-methylthiose-micarbazone (*Cu-ATSM) [6–8], and ^{124}I-labeled iodoazomycin galactopyranoside (^{124}I-IAZGP) [9–11] amongst others are under investigation for in vivo PET imaging of tumor hypoxia. Although noninvasive PET imaging may be impractical for directly assessing hypoxia in microscopic tumors which are too small to be seen [2], such models may provide a useful means of corroborating the validity of purported hypoxia tracers. There are powerful methods of assessing the microenvironmental features of individual microscopic tumors, including their hypoxic status, and relating these to the uptake of radiolabeled tracer. In addition, such models provide a diversity of tumors of differing size and hypoxic status growing in the same animal, thereby reducing or eliminating issues associated with inter-animal variability.

The exogenous hypoxia marker pimonidazole is a 2-nitroimidazole compound that is selectively reduced in hypoxic regions (generally pO_2 <10 mmHg) of tumors, subsequently binding to intracellular macromolecules [12]. Pimonidazole has been widely used in clinical and experimental studies of tumor hypoxia [1,8,13–17]. Proteins regulated by hypoxia through the HIF pathway can be used as endogenous hypoxia markers. Examples include carbonic anhydrase IX (CAIX) and glucose transporter-1 (GLUT-1) [18–21] and there are many others [22]. The spatial distributions of pimonidazole binding and upregulated expression of proteins such as CAIX can be visualized on tumor sections by immunohistochemical methods [23]. Although CAIX may not be useful in all tumor models [24], we have observed spatial co-

localization of pimonidazole binding and enhanced CAIX expression in both macroscopic and microscopic HT29 tumors, implying that CAIX is a useful marker of hypoxia in this model [1,2,25]. In addition to hypoxia, the spatial distributions of other aspects of the tumor microenvironment such as vascularity, blood perfusion, and cellular proliferation can be visualized on tumor tissue sections by appropriate means.

To complement the high spatial resolution associated with immunohistochemical detection of hypoxia markers, the intratumoral distribution of radiolabeled hypoxia tracers can be determined by autoradiographic means. Digital autoradiographic (DAR) detection systems can determine the spatial distribution of activity in a quantitative manner with pixel resolutions of 25–50 μm. Studies comparing the spatial distributions of radiolabeled tracers and immunohistochemically detected hypoxia markers in macroscopic tumors have been reported previously [8,26]; however, these methods have not yet been applied to models of microscopic disease.

In this study, we report for the first time the use of correlative imaging methods to examine the distribution of a radiolabeled hypoxia tracer (^{131}I-IAZGP) in microscopic tumors and relate this to hypoxic status as determined by pimonidazole and CAIX immunohistochemistry.

Materials and methods

Cancer cell line and animals

The human colorectal adenocarcinoma cell line HT29 was purchased from American Type Cell Collection (Manassas, VA, USA). HT29 cells were maintained in McCoy's 5A modified medium (Gibco, Grand Island, NY, USA) supplemented with 10% fetal bovine serum (Gemini, West Sacramento, CA, USA), 1% glutamine, and 1% antibiotic mixture (Cellgro, Manassas, VA, USA). Cells were grown at 37°C in a humidified CO_2 incubator. Exponentially growing cells were harvested with 0.05% trypsin *plus* ethylenediaminetetraacetate (EDTA) (Cellgro, Manassas, VA, USA), washed, and suspended in phosphate-buffered saline (PBS). The number of cells was counted using a Coulter counter (Beckman-Coulter, Miami, FL, USA).

All experiments were performed using 6- to 8-week-old female athymic NCr-*nu/nu* mice purchased from NCI-Frederick Cancer Research Institute (Bethesda, MD, USA). Nude mice were maintained and used according to institutional guidelines. The experimental protocols were approved by the Institutional Animal Care and Use Committee. Animals were housed five per cage and kept in the institutional small animal facility at a constant temperature and humidity. Food pellets and water were provided ad libitum.

Establishment of tumors in animals

Microscopic peritoneal tumors—Disseminated microscopic tumors were induced in the peritoneum by injecting HT29 tumor cell suspensions (10^7 cells/0.2 ml) into the peritoneal cavity. Animals (five mice) were sacrificed 6–7 weeks after tumor cell administration. At this time, a distribution of tumors ranging from a few hundred micrometers up to several millimeters in diameter was observed to be present on or in the intestinal serosa.

Ascites tumors—At the time of sacrifice, ascites was evident in the majority of animals. The ascites fluid was observed to be bloody and contained a distribution of free-floating tumor cell aggregates of sizes up to 1 mm in diameter, denoted here as *ascites tumors*. Ascites tumors were typically ellipsoidal in shape with a “rough” surface and the appearance of duct-like structures in the interior.

Microscopic intradermal tumors—HT29 cell suspensions containing 2.5×10^5 (4 μl), 5×10^5 (8 μl), 10^6 (16 μl), or 2×10^6 (32 μl) cells were injected using a 100-μl syringe (Hamilton, Reno, NV, USA) into four mice at four intradermal sites per animal and allowed to grow for 3–7 days. Tumor sizes were dependent on the number of cells injected at the time of assay and ranged from a few hundred micrometers to several millimeters in diameter.

Labeling IAZGP with ^{131}I

IAZGP was labeled with ^{131}I by an I-^{131}I exchange reaction according to the method of Schneider et al. [27] with some modifications [28]. Briefly, 5–7 μl of $Na^{131}I$/0.1 N NaOH (11–37 GBq/ml, PerkinElmer, Waltham, MA, USA) was transferred into a 0.1-ml Reacti-Vial (Pierce, Rockford, IL, USA), to which 50 μl of anhydrous ethanol was added. The solvent was evaporated under a stream of N_2. This step was repeated until dry $Na^{131}I$ was obtained. To the dried residue, 1 mg of unlabeled IAZGP in 20 μl of dimethyl-formamide (DMF) was added, and the reaction mixture heated at 82–86°C for 5 h. The solvent was evaporated and the residue dissolved in 0.2 ml of water, which was passed through an anion exchange column (AG1X8, 200–400 mesh, approximately 40 mg). The eluant was passed through a 0.22-μm Millex filter (Millipore, Bedford, MA, USA) and collected in a 1-ml vial. For quality control (QC) purposes, an aliquot of the final product was applied to a C18 HPLC analytical column (NovaPak 4.6 × 250 mm, Alltech, Deerfield, IL, USA) and eluted with acetonitrile/water (10/90) at a flow rate of 2 ml/min. Under these conditions, the retention time of IAZGP was 7.5 min. Overall radiochemical yields of ^{131}I-IAZGP were 56±5% and the total synthesis time was 7.3±0.3 h. Radiochemical purity was 100%.

Administration of ^{131}I-IAZGP, pimonidazole, and Hoechst 33342

The hypoxic cell marker pimonidazole hydrochloride (1-[(2-hydroxy-3-piperidinyl)propyl]-2-nitroimidazole hydrochloride) (Chemicon International, Temecula, CA, USA) was dissolved in physiological saline. A 0.2 ml mixture containing ^{131}I-IAZGP (3.7 MBq) and pimonidazole (2 mg) was administrated to tumor-bearing nude mice via tail vein 2 h before sacrifice. The fluorescent dye Hoechst 33342 (Sigma-Aldrich, St. Louis, MO, USA, 0.5 mg in 0.1 ml physiological saline) was injected 1 min before sacrifice.

Preparation of frozen tumor sections

Immediately after animal sacrifice, tumor tissues or ascites fluid were removed for subsequent processing. Intradermal tumors were immediately dissected, frozen on dry ice, and embedded in optimal cutting tissue compound (OCT. 4583, Sakura Finetek, Torrance, CA, USA). Peritoneal tumors were washed with PBS to remove any attached ascitic cancer cells before freezing and embedding in OCT. Ascites tumors were harvested, washed with cold PBS (4°C) to remove red blood cells, frozen, and embedded in OCT. For all tumor samples, sets of five contiguous 8-μm thick tissue sections were cut using a Microm HM500 cryostat microtome (Microm International GmbH, Walldorf, Germany) and adhered to poly-L-lysine coated glass microscope slides.

^{131}I-IAZGP digital autoradiography

Autoradiograms were obtained by placing tumor tissue sections in a film cassette against a Fujifilm BAS-MS2325 imaging plate (Fuji Photo Film Co., Tokyo, Japan). The plate was exposed for a fixed time period of 20 h and then read by a Fujifilm BAS-1800II bio-imaging analyzer (Fuji Photo Film Co., Tokyo, Japan) which generated digital images with pixel dimensions of 50 × 50 μm. The same plate was used for all experiments. DAR image intensity was expressed in the machine readout parameter of photo-stimulable luminescence per square mm (PSL/mm^2) and was quantified using Multi Gauge software (version 2.2, Fujifilm). Subsequently the derived PSL/mm^2 values were converted to MBq/g based on the known start

and end times of the DAR exposure and a previously measured system calibration factor of 103 PSL/mm^2 per MBqh/g. Finally tumor uptakes were expressed in terms of percentage injected dose per gram based on the known administered activities.

Visualization of pimonidazole, CAIX, Hoechst 33342, and hematoxylin and eosin (H&E) on tumor sections

Images of the distributions of pimonidazole, CAIX, and Hoechst 33342 were obtained from tumor sections after completion of ^{131}I-IAZGP DAR exposures. In order to minimize issues associated with section alignment and registration, wherever possible the same tumor section was used for all images at a given location.

As described previously [1], slides were fixed in cold acetone (4°C) for 20 min and incubated with SuperBlock (Pierce Biotechnology, Rockford, IL, USA) at room temperature for 30 min. All antibodies were also applied in SuperBlock. Sections were then incubated with fluorescein isothiocyanate (FITC)-conjugated anti-pimonidazole monoclonal antibody (Chemicon International, Temecula, CA, USA), diluted 1:25, for 1 h at room temperature. Tumor sections were co-stained for CAIX by including chimeric anti-CAIX antibody (cG250) (a gift from Dr. Gerd Ritter, Ludwig Institute for Cancer Research, New York, NY, USA) at a final concentration of 10 μg/ml. Sections were washed three times in PBS, each wash lasting 5 min, incubated with AlexaFluor568-conjugated goat anti-human antibody (20 μg/ml, Molecular Probes, Eugene, OR, USA) for 1 h at room temperature, and washed again. Images were acquired at×100 magnification using an Olympus BX40 fluorescence microscope (Olympus America Inc., Melville, NY, USA) equipped with a motorized stage (Prior Scientific Instruments Ltd., Cambridge, UK). Hoechst 33342, pimonidazole, and CAIX were imaged using blue, green, and red filters, respectively. To control for nonspecific binding of antibodies, stained sections were processed from similar tumors that had not been exposed to pimonidazole. Controls for CAIX staining consisted of sections where primary antibody was omitted.

After acquisition of fluorescence images, the same or adjacent contiguous tumor sections were stained with H&E and imaged by light microscopy to identify viable and necrotic tumor tissue. All images were co-registered and analyzed using Adobe Photoshop 7.0 (Adobe, San Jose, CA, USA). Statistical significance was examined by two-tailed Student's *t* test

Results

The distributions of ^{131}I-IAZGP, pimonidazole, and CAIX were examined in conjunction with perfusion (Hoechst 33342) and morphology (H&E). Figure 1 shows an example of the intratumoral distributions of ^{131}I-IAZGP, pimonidazole binding, and CAIX expression in a small (~1 mm dimension) and relatively large tumor obtained from an animal with disseminated peritoneal disease. The smaller tumor shows elevated uptake of ^{131}I-IAZGP and near-ubiquitous staining of pimonidazole and CAIX, implying almost uniform hypoxia. This is consistent with the low Hoechst 33342 uptake which indicates that this tumor was poorly perfused. The larger tumor shows reduced ^{131}I-IAZGP uptake and low levels of pimonidazole binding and CAIX expression together with significant Hoechst 33342 uptake indicating that the tumor was well-perfused. Also shown is quantitative ^{131}I-IAZGP uptake in a collection of 27 intraperitoneal tumors of greater or less than 1 mm diameter from the same animal indicating significantly higher uptake in submillimeter tumors.

Figure 2 shows DAR and immunofluorescence images of microscopic ascites tumors from an animal with disseminated peritoneal disease indicating high ^{131}I-IAZGP uptake coupled with intense staining of pimonidazole and CAIX. These tumors were completely negative for Hoechst 33342 (data not shown). The histogram shows a statistically significant difference

in ^{131}I-IAZGP uptake between ascites tumors (n=4) and intraperitoneal tumors of less than 1 mm diameter (n=4) and larger intraperitoneal tumors (n=5) from a single animal. ^{131}I-IAZGP uptake between ascites tumors and intraperitoneal tumors (<1 mm diameter) is not significantly different.

Figure 3 shows images of smaller (a) and larger (b) intradermal tumors. The smaller tumor (< 1 mm in diameter) was characterized by a central lack of blood perfusion, high levels of co-localized pimonidazole binding and CAIX expression, and high ^{131}I-IAZGP accumulation. In contrast, intradermal tumors above 1 mm in diameter were well perfused, had low ^{131}I-IAZGP and pimonidazole accumulation, and had low CAIX expression. ^{131}I-IAZGP uptake was quantified in 11 HT29 intradermal tumors from various animals. Uptake was significantly higher in microscopic tumors (<1 mm diameter, n=5) than larger ones (>1 mm, n=6), p<0.001

Discussion

We have previously reported the existence of severe hypoxia in microscopic tumors derived from HT29 colorectal cancer cells grown intraperitoneally and intradermally in nude mice [1]. The current study confirms these findings and extends them to include the use of radiolabeled hypoxia tracers as a means of verification. In this regard, an important advantage of the radiotracer methodology is the ability to quantify uptake and thereby derive statistically meaningful interpretations of the differences between smaller and larger tumors. Such interpretations are less straightforward with immunofluorescence methods as the linearity of fluorescence intensity as a metric is not established. Nevertheless, in all cases examined there was a clear qualitative agreement between the results of ^{131}I-IAZGP uptake and those based on the immunofluorescent visualization of pimonidazole binding. We anticipate that this correspondence should extend to models based on other tumor cell lines as essentially all that is being compared is the uptake of two relatively similar 2-nitroimidazole species administered intravenously. We also observed a qualitative agreement between ^{131}I-IAZGP uptake and immunofluorescent visualization of enhanced expression of the hypoxia-induced protein CAIX. This is much less likely to be universally applicable as the spectrum of protein expression is a more idiosyncratic function of phenotype. Indeed in HCT-8-derived tumors we could not visualize CAIX expression under any circumstances [1]. What is more likely is that there will be a correspondence between a hypoxic radiotracer and enhanced expression of some hypoxia-regulated protein or proteins, the identity of which may vary from cell line to cell line.

The second aspect of these findings that deserves comment is that the microscopic tumor model, especially the disseminated intraperitoneal case, is a useful system for the development and validation of radiolabeled hypoxia tracers for clinical applications. Microscopic tumors of submillimeter dimensions were severely hypoxic as judged by high levels of pimonidazole binding and CAIX expression, and indirectly by the absence of blood perfusion. Invariably, these tumors had high ^{131}I-IAZGP accumulation. Conversely, tumors between ~1 and ~4 mm in diameter were not significantly hypoxic, based on the observation of little pimonidazole binding or CAIX expression. These tumors had low ^{131}I-IAZGP accumulation. Thus, differences in uptake of some purported hypoxia radiotracer between these different classes of microscopic tumors may be a useful guide to the hypoxic selectivity of the radiotracer. We have shown that digital autoradiography is a suitable means to study radiotracer uptake in microscopic tumors.

In this study IAZGP was labeled with ^{131}I, primarily for reasons of costs and practicality. The positron emitting ^{124}I would obviously be the isotope of choice for PET imaging studies [10] and it could be reasonably argued that ^{125}I would be a more ideal radiolabel for autoradiography due to its lower energy (and thus shorter range) emissions. However ^{124}I is cyclotron-produced,

expensive, and for a non-PET imaging study unnecessary, while the use of ^{125}I with its long half-life (60 days) is problematic from a radiation safety perspective.

Previous studies have shown that having animals breathe carbogen gas (95% O_2, 5% CO_2) can reduce hypoxia in microscopic tumors [1]. However, in the current study we did not attempt to observe the effect of breathing gas mixtures with differing oxygen concentration on ^{131}I-IAZGP uptake. This will be examined in a future study.

Disseminated peritoneal disease as a test system for radiotracer validation has several advantages compared with macroscopic subcutaneous xenografts. Individual small tumors have an approximately homogeneous internal structure, being either hypoxic and unperfused, or non-hypoxic and well perfused. This makes it relatively simple to demonstrate co-localization of radiotracer (DAR) and hypoxia marker (immunofluorescence). In contrast, macroscopic xenografts have a complex internal structure with intermingled regions of normal stroma, well oxygenated tumor, hypoxia, and necrosis in close proximity. Consequently, when comparing DAR and immunofluorescence images in macroscopic xenografts, problems of interpretation may arise due to uncertainties in image matching. Another advantage is that since hundreds of intraperitoneal tumors of various sizes and degrees of hypoxia can exist in an individual animal, it is possible to compare radiotracer uptake between tumors without confounding variations due to differences in injected dose or inter-animal pharmaco-kinetics. Therefore, the disseminated peritoneal disease model is, at least, a valuable supplement to macroscopic xenograft models as a test system for radiotracer development.

The microscopic tumor model may also be useful in the study of the metastatic process, as such tumors growing in animals may mimic some aspects of micrometastatic disease in patients. In particular, if the pre-angiogenic phase of micrometastatic development involves an episode of severe hypoxia similar to that seen here, the efficacy of adjuvant/neoadjuvant treatment may be compromised by hypoxic resistance [1,2]. Should this be the case, new approaches to systemic treatment that specifically target hypoxia may be necessary.

There are a variety of proposed methods for targeting the different manifestations of the hypoxia phenotype that may be relevant in this context [29,30]. Preliminary studies with the hypoxia-selective cytotoxin tirapazamine were encouraging [31–33]; however, the experience in large-scale clinical studies has been disappointing to date [34]. Alternative hypoxic cytotoxins that may represent improvements on tirapazamine are in earlier stages of investigation [35–37]. These types of drug rely on the hypoxia-induced bioreduction of a prodrug to an active form. Other groups are investigating the potential of recombinant anaerobic bacteria [38,39] that become active only in regions of very low pO_2 and may be directly oncolytic or vectors for the delivery of therapeutic genes. Another possibility is to target the HIF-1 signal transduction pathway, and a variety of approaches aimed at either inhibition of HIF-1 activation or HIF-1 target genes are under investigation (reviewed in [30]). To this list, one could speculatively add the possibility of a therapeutic variant of a hypoxia imaging tracer. For example, a hypoxia-selective molecule labeled with an alpha particle emitting radionuclide with a relatively short half-life (such as ^{213}Bi or ^{211}At) may be attractive since the cytotoxic effect of alpha particles is not modified by the absence of oxygen [40]. Of course the utility of such an agent would depend on its biodistribution and comparative (tumor versus normal tissues) dosimetry. This suggests there could be particular applicability to disseminated disease in confined body regions, such as the peritoneal cavity, where there would be restricted transfer to the systemic circulation.

Conclusion

We have used ^{131}I-IAZGP to detect hypoxia in microscopic tumors derived from the HT29 colorectal cancer cell line grown intraperitoneally and intradermally in nude mice. Such tumor

models are useful for validating current and novel hypoxia tracers. Digital autoradiography is an appropriate technique for studying the distribution of radiolabeled hypoxia tracers in microscopic tumors.

Acknowledgments

National Institute of Health grants R01 CA84596 and P01 CA115675, National Cancer Institute grant P30-CA 08748.

References

1. Li XF, Carlin S, Urano M, Russell J, Ling CC, O'Donoghue JA. Visualization of hypoxia in microscopic tumors by immunofluorescent microscopy. Cancer Res 2007;67:7646–53. [PubMed: 17699769]
2. Li XF, O'Donoghue JA. Hypoxia in microscopic tumors. Cancer Lett 2008;264:172–80. [PubMed: 18384940]
3. Bentzen L, Keiding S, Horsman MR, Falborg L, Hansen SB, Overgaard J. Feasibility of detecting hypoxia in experimental mouse tumours with 18F-fluorinated tracers and positron emission tomography—a study evaluating [18F]fluoro-2-deoxy-D-glucose. Acta Oncol 2000;39:629–37. [PubMed: 11093372]
4. Dubois L, Landuyt W, Haustermans K, Dupont P, Bormans G, Vermaelen P, et al. Evaluation of hypoxia in an experimental rat tumour model by [(18)F]fluoromisonidazole PET and immunohistochemistry. Br J Cancer 2004;91:1947–54. [PubMed: 15520822]
5. He F, Deng X, Wen B, Liu Y, Sun X, Xing L, et al. Noninvasive molecular imaging of hypoxia in human xenografts: comparing hypoxia-induced gene expression with endogenous and exogenous hypoxia markers. Cancer Res 2008;68:8597–606. [PubMed: 18922936]
6. Vāvere AL, Lewis JS. Cu-ATSM: a radiopharmaceutical for the PET imaging of hypoxia. Dalton Trans 2007;43:4893–902. [PubMed: 17992274]
7. Tatum JL, Kelloff GJ, Gillies RJ, Arbeit JM, Brown JM, Chao KS, et al. Hypoxia: importance in tumor biology, noninvasive measurement by imaging, and value of its measurement in the management of cancer therapy. Int J Radiat Biol 2006;82:699–757. [PubMed: 17118889]
8. O'Donoghue JA, Zanzonico P, Pugachev A, Wen B, Smith-Jones P, Cai S, et al. Assessment of regional tumor hypoxia using 18F-fluoromisonidazole and 64Cu(II)-diacetyl-bis(N4-methylthiosemicarbazone) positron emission tomography: comparative study featuring microPET imaging, Po2 probe measurement, autoradiography, and fluorescent microscopy in the R3327-AT and FaDu rat tumor models. Int J Radiat Oncol Biol Phys 2005;61:1493–502. [PubMed: 15817355]
9. Iyer RV, Engelhardt EL, Stobbe CC, Schneider RF, Chapman JD. Preclinical assessment of hypoxic marker specificity and sensitivity. Int J Radiat Oncol Biol Phys 1998;42:741–5. [PubMed: 9845088]
10. Zanzonico P, O'Donoghue J, Chapman JD, Schneider R, Cai S, Larson S, et al. Iodine-124-labeled iodo-azomycin-galactoside imaging of tumor hypoxia in mice with serial microPET scanning. Eur J Nucl Med Mol Imaging 2004;31:117–28. [PubMed: 14523586]
11. Riedl CC, Brader P, Zanzonico PB, Chun YS, Woo Y, Singh P, et al. Imaging hypoxia in orthotopic rat liver tumors with iodine 124-labeled iodoazomycin galactopyranoside PET. Radiology 2008;248:561–70. [PubMed: 18641253]
12. Ljungkvist AS, Bussink J, Kaanders JH, van der Kogel AJ. Dynamics of tumor hypoxia measured with bioreductive hypoxic cell markers. Radiat Res 2007;167:127–45. [PubMed: 17390721]
13. Sun X, Li XF, Russell J, Xing L, Urano M, Li GC, et al. Changes in tumor hypoxia induced by mild temperature hyperthermia as assessed by dual-tracer immunohistochemistry. Radiother Oncol 2008;88:269–76. [PubMed: 18538874]
14. Kaanders JH, Wijffels KI, Marres HA, Ljungkvist AS, Pop LA, van den Hoogen FJ, et al. Pimonidazole binding and tumor vascularity predict for treatment outcome in head and neck cancer. Cancer Res 2002;62:7066–74. [PubMed: 12460928]
15. Raleigh JA, Calkins-Adams DP, Rinker LH, Ballenger CA, Weissler MC, Fowler WC Jr, et al. Hypoxia and vascular endothelial growth factor expression in human squamous cell carcinomas using pimonidazole as a hypoxia marker. Cancer Res 1998;58:3765–8. [PubMed: 9731480]

16. Raleigh JA, Chou SC, Arteel GE, Horsman MR. Comparisons among pimonidazole binding, oxygen electrode measurements, and radiation response in C3H mouse tumors. Radiat Res 1999;151:580–9. [PubMed: 10319731]

17. Ljungkvist AS, Bussink J, Rijken PF, Raleigh JA, Denekamp J, Van Der Kogel AJ. Changes in tumor hypoxia measured with a double hypoxic marker technique. Int J Radiat Oncol Biol Phys 2000;48:1529–38. [PubMed: 11121659]

18. Driessen A, Landuyt W, Pastorekova S, Moons J, Goethals L, Haustermans K, et al. Expression of carbonic anhydrase IX (CA IX), a hypoxia-related protein, rather than vascular-endothelial growth factor (VEGF), a pro-angiogenic factor, correlates with an extremely poor prognosis in esophageal and gastric adenocarci-nomas. Ann Surg 2006;243:334–40. [PubMed: 16495697]

19. Hoskin PJ, Sibtain A, Daley FM, Wilson GD. GLUT1 and CAIX as intrinsic markers of hypoxia in bladder cancer: relationship with vascularity and proliferation as predictors of outcome of ARCON. Br J Cancer 2003;89:1290–7. [PubMed: 14520462]

20. Potter CP, Harris AL. Diagnostic, prognostic and therapeutic implications of carbonic anhydrases in cancer. Br J Cancer 2003;89:2–7. [PubMed: 12838292]

21. Koukourakis MI, Giatromanolaki A, Sivridis E, Simopoulos K, Pastorek J, Wykoff CC, et al. Hypoxia-regulated carbonic anhydrase-9 (CA9) relates to poor vascularization and resistance of squamous cell head and neck cancer to chemoradiotherapy. Clin Cancer Res 2001;7:3399–403. [PubMed: 11705854]

22. Harris AL. Hypoxia—a key regulatory factor in tumour growth. Nat Rev Cancer 2002;2:38–47. [PubMed: 11902584]

23. Sobhanifar S, Aquino-Parsons C, Stanbridge EJ, Olive P. Reduced expression of hypoxia-inducible factor-1alpha in perinecrotic regions of solid tumors. Cancer Res 2005;65:7259–66. [PubMed: 16103077]

24. Troost EG, Bussink J, Kaanders JH, van Eerd J, Peters JP, Rijken PF, et al. Comparison of different methods of CAIX quantification in relation to hypoxia in three human head and neck tumor lines. Radiother Oncol 2005;76:194–9. [PubMed: 16024110]

25. Shin KH, Diaz-Gonzalez JA, Russell J, Chen Q, Burgman P, Li XF, et al. Detecting changes in tumor hypoxia with carbonic anhydrase IX and pimonidazole. Cancer Biol Ther 2007;6:70–5. [PubMed: 17172824]

26. Pugachev A, Ruan S, Carlin S, Larson SM, Campa J, Ling CC, et al. Dependence of FDG uptake on tumor microenvironment. Int J Radiat Oncol Biol Phys 2005;62:545–53. [PubMed: 15890599]

27. Schneider RF, Engelhardt EL, Stobbe CC, Fenning MC, Chapman JD. The synthesis and radiolabelling of novel markers of tissue hypoxia of the iodinated azomycin nucleoside class. J Labelled Compd Radiopharm 1997;39:541–57.

28. Suehiro M, Burgman P, Carlin S, Burke S, Yang GB, Ouerfelli O, et al. Radiosynthesis of [(131)I] IAZGP via nucleophilic substitution and its biological evaluation as a hypoxia marker—is specific activity a factor influencing hypoxia-mapping ability of a hypoxia marker? Nucl Med Biol 2009;36:477–87. [PubMed: 19520288]

29. Brown JM, Wilson WR. Exploiting tumour hypoxia in cancer treatment. Nat Rev Cancer 2004;4:437–47. [PubMed: 15170446]

30. Melillo G. Targeting hypoxia cell signaling for cancer therapy. Cancer Metastasis Rev 2007;26:341–52. [PubMed: 17415529]

31. Denny WA, Wilson WR. Tirapazamine: a bioreductive anticancer drug that exploits tumour hypoxia. Expert Opin Investig Drugs 2000;9:2889–901.

32. von Pawel J, von Roemeling R, Gatzemeier U, Boyer M, Elisson LO, Clark P, et al. Tirapazamine plus cisplatin versus cisplatin in advanced non-small-cell lung cancer: a report of the international CATAPULT I study group. Cisplatin and tirapazamine in subjects with advanced previously untreated non-small-cell lung tumors. J Clin Oncol 2000;18:1351–9. [PubMed: 10715308]

33. Rischin D, Hicks RJ, Fisher R, Binns D, Corry J, Porceddu S, et al. Prognostic significance of [18F]-misonidazole positron emission tomography-detected tumor hypoxia in patients with advanced head and neck cancer randomly assigned to chemoradiation with or without tirapazamine: a substudy of Trans-Tasman Radiation Oncology Group Study 98.02. J Clin Oncol 2006;24:2098–104. [PubMed: 16648512]

34. Reddy SB, Williamson SK. Tirapazamine: a novel agent targeting hypoxic tumor cells. Expert Opin Investig Drugs 2009;18:77–87.

35. Lalani AS, Alters SE, Wong A, Albertella MR, Cleland JL, Henner WD. Selective tumor targeting by the hypoxia-activated prodrug AQ4N blocks tumor growth and metastasis in preclinical models of pancreatic cancer. Clin Cancer Res 2007;13:2216–25. [PubMed: 17404106]

36. Patterson AV, Ferry DM, Edmunds SJ, Gu YC, Singleton RS, Patel K, et al. Mechanism of action and preclinical antitumor activity of the novel hypoxia-activated DNA cross-linking agent PR-104. Clin Cancer Res 2007;13:3922–32. [PubMed: 17606726]

37. Duan JX, Jiao H, Kaizerman J, Stanton T, Evans JW, Lan L, et al. Potent and highly selective hypoxia-activated achiral phosphoramidate mustards as anticancer drugs. J Med Chem 2008;51:2412–20. [PubMed: 18257544]

38. Pawelek JM, Low KB, Bermudes D. Bacteria as tumour-targeting vectors. Lancet Oncol 2003;4:548–56. [PubMed: 12965276]

39. Wei MQ, Mengesha A, Good D, Anné J. Bacterial targeted tumour therapy-dawn of a new era. Cancer Lett 2008;259:16–27. [PubMed: 18063294]

40. Mulford DA, Scheinberg DA, Jurcic JG. The promise of targeted {alpha}-particle therapy. J Nucl Med 2005;46(Suppl 1):199S–204S. [PubMed: 15653670]

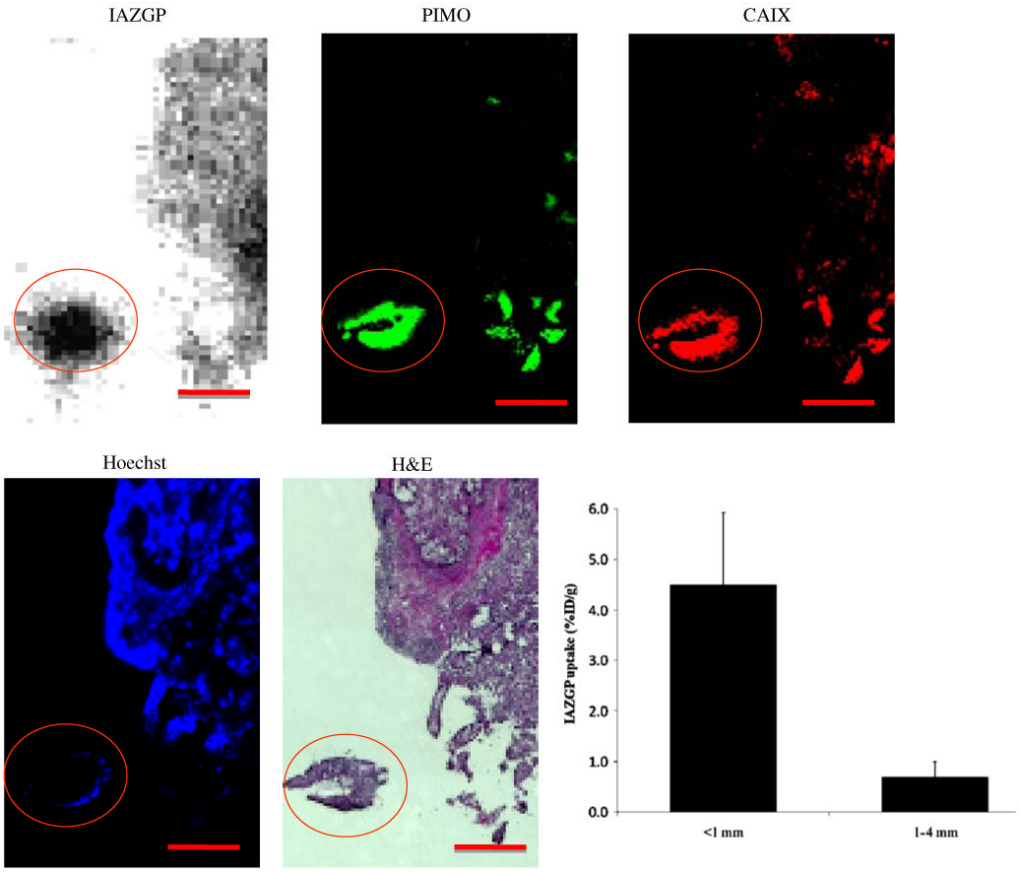

Fig. 1.

Comparison of intratumoral distribution of ^{131}I-IAZGP with pimonidazole binding (*green*), hypoxia-regulated protein CAIX (*red*), and Hoechst 33342 (*blue*) in a tissue section containing disseminated intraperitoneal (i.p.) HT29 tumors. A larger tumor, part of which is seen in the upper right quadrant has low levels of ^{131}I-IAZGP uptake, pimonidazole binding, and CAIX expression together with significant blood perfusion. The microscopic tumor with dimensions of ~1 mm (*circled*) has high ^{131}I-IAZGP uptake throughout the tumor together with high pimonidazole binding and CAIX expression. All images were obtained from the same tissue section. *Scale bar* =1 mm. The histogram shows quantitative ^{131}I-IAZGP uptake in a collection of 27 i.p. HT29 tumors from a single animal expressed as % injected dose per gram. Tumor uptake was derived from an ^{131}I-IAZGP autoradiograph with individual tumor sizes based on the H&E image. ^{131}I-IAZGP uptake was significantly higher in microscopic i.p. tumors (<1 mm diameter, n=18) than larger ones (>1 mm, n=9), p<0.001

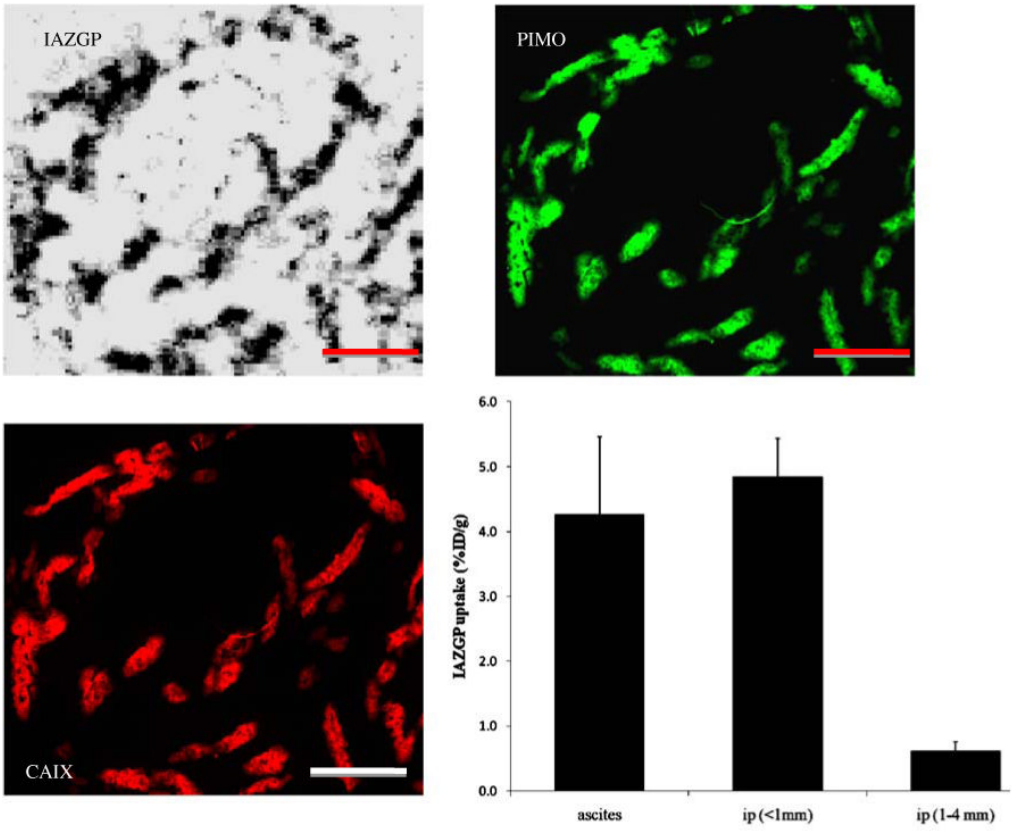

Fig. 2.

High levels of ^{131}I-IAZGP uptake, pimonidazole binding, and CAIX expression in HT29 ascites tumors from a single animal. *Scale bar*=1 mm. The histogram shows quantitative ^{131}I-IAZGP uptake in a collection of 13 ascites and intraperitoneal (i.p.) tumors from a single animal. Uptake in ascites and smaller i.p. tumors was significantly higher than in larger tumors, $p<0.001$

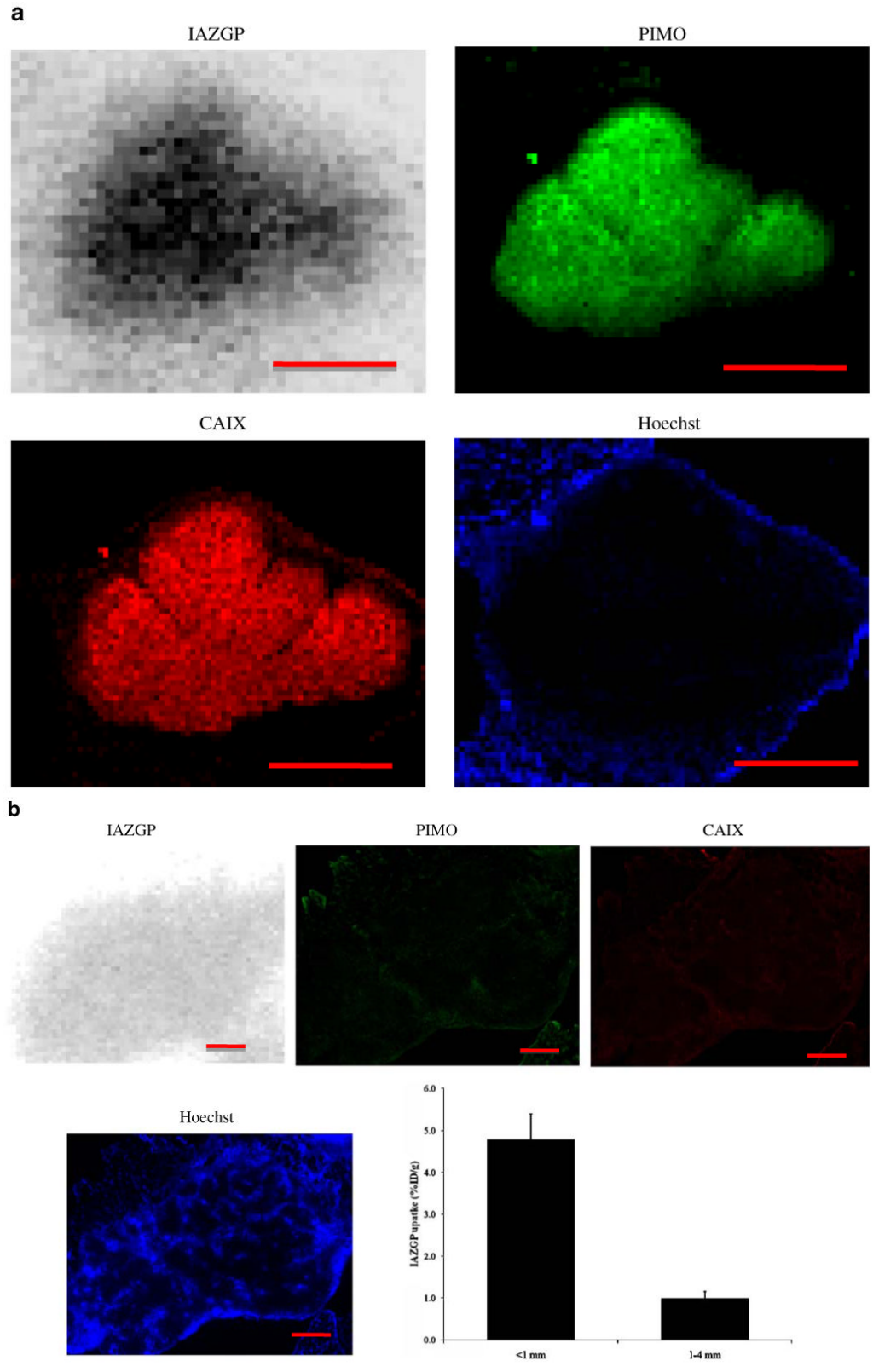

Fig. 3.

Comparison of intratumoral distribution of ^{131}I-IAZGP uptake, pimonidazole binding, CAIX expression, and blood perfusion in a microscopic and a larger HT29 intradermal (i.d.) tumor. The microscopic tumor (**a**) shows high ^{131}I-IAZGP uptake, pimonidazole binding, and CAIX expression with little to no blood perfusion. The larger tumor (**b**) shows the complete opposite in all respects. *Scale bar*=500μm. The histogram (**b**) shows a summary of quantitative ^{131}I-IAZGP uptake in 11 HT29 i.d. tumors from a variety of animals. ^{131}I-IAZGP uptake was significantly higher in microscopic i.d. tumors (<1 mm diameter, n=5) than larger ones (>1 mm, n=6), p<0.001